

Article

Dissolution Kinetics of Chlorine from Iron Ore Sintering Dust

Honghu Tang^{1,2}, Lihua Zhao³, Yue Yang^{1,2} , Haisheng Han^{1,2}, Li Wang^{1,2,*}  and Wei Sun^{1,2}

¹ School of Minerals Processing and Bioengineering, Central South University, Changsha 410083, China; honghu.tang@csu.edu.cn (H.T.); eric1911@126.com (Y.Y.); hanhaishengjingji@126.com (H.H.); sunmenghu@csu.edu.cn (W.S.)

² Key Laboratory of Hunan Province for Clean and Efficient Utilization of Strategic Calcium-Containing Mineral Resources, Central South University, Changsha 410083, China

³ Hunan Zhongye Changtian Energy Conservation and Environment Protection Technology Co., Ltd., Changsha 410205, China; zhaolihua152@126.com

* Correspondence: li_wang@csu.edu.cn; Tel.: +86-731-8887-6697

Abstract: Chlorine is generated during iron ore sintering, mostly in the form of alkali chlorides and primarily accumulates in sintering dust, which must be removed before reusing. In this study, an in-situ monitor leaching system based was designed to detect chloride ion water leaching behaviors in real-time and improve the understanding of chlorine dissolution kinetic behaviors in water. Various parameters, including water leaching temperature, solid/liquid ratio, stirring speed, particle size and surfactant addition have been studied. Meanwhile their chlorine dissolution data exhibited a good fit to Stumm's kinetic models. The results of kinetics analysis and transition state theory calculation on apparent activation energy demonstrated that the dissolution process was controlled by diffusion at low S/L ratio, while changed to be controlled by surface chemical reaction as the S/L ratio increased. Furthermore, increasing both temperature and stirring speed improved the chlorine removal speed. Moreover, reducing the particle size and adding 0.2% nonionic surfactant Triton X-100 reduced the surface energy and accelerated surface chemical reaction, which were also beneficial for removing chlorine from sintering dust. In addition, the SEM-EDS examination inferred that the existence of laurionite (PbOHCl) limited the chlorine dissolution rate to less than 97%, while beneficiation or hydrometallurgy treatment was needed to further remove chlorine.

Keywords: iron ore sintering dust; dissolution kinetics; Stumm's kinetic model; chlorine removing; surfactant addition



Citation: Tang, H.; Zhao, L.; Yang, Y.; Han, H.; Wang, L.; Sun, W. Dissolution Kinetics of Chlorine from Iron Ore Sintering Dust. *Metals* **2021**, *11*, 1185. <https://doi.org/10.3390/met11081185>

Academic Editors:
Eleazar Salinas-Rodríguez and Jean François Blais

Received: 23 April 2021
Accepted: 10 July 2021
Published: 26 July 2021

Publisher's Note: MDPI stays neutral with regard to jurisdictional claims in published maps and institutional affiliations.



Copyright: © 2021 by the authors. Licensee MDPI, Basel, Switzerland. This article is an open access article distributed under the terms and conditions of the Creative Commons Attribution (CC BY) license (<https://creativecommons.org/licenses/by/4.0/>).

1. Introduction

Iron ore sintering is an essential processing step in modern integrated iron and steel making process, which produced over 60% of the global crude steel [1,2]. During this procedure, sintering dust was generated and then collected by electrostatic precipitator, which accounts for approximately 40% of the total emission in the iron and steel industry [3]. It has a production about 28 to 45 kg per ton of steel, as evaluated by previous data [4], meanwhile it is also considered as a kind of hazardous waste because of its complicated components such as chlorides, heavy metals and dangerous organics [5]. As one of the main solid wastes of iron and steel plants, the treatment of sintering dust is still a headache of a steel plant [6,7]. Recycling this waste materials back into the iron ore sintering process is a general disposal approach worldwide. However, the high contents of harmful components, particularly chlorides, in this dust would cause serious difficulties in sintering, which makes directly recycle sintering dust still a thorny problem [8]. Furthermore, chlorides, as the main chlorine sources in sintering dust, is one of the key factors for the formation of PCDD/Fs during iron ore sintering process [2,9]. Therefore, it is of great importance to improve chlorides removal efficiency from the sintering dust, as it will not only benefit the recycling of this material back into the sintering process but also help reducing the dioxin emission during its reuse.

However, most of the previous studies only removed the chlorine as a side-effect of extracting potassium from iron ore sintering dust in the form of KCl [7], while the investigation of chlorine removal was neglected. The chlorine mainly exists in the form of chlorides such as KCl, NaCl, ZnCl₂, PbOHCl, etc. in sintering dust [10]. The formation of chlorides is due to their low boiling points [11,12] and high partial pressures [8,13] during the sintering process. Water leaching, fractional crystallization, solvent extraction was employed to recover K and Rb from sintering dust [14,15]. Some of the Cl will also be removed from the sintering dust during these treatments, however, the leaching behavior and kinetics on chlorine removing is still unclear. Lack of sensitive in-situ analysis method of chlorine in solution was one of the difficulties, since the commonly used inductively coupled plasma or ion exchange chromatography were not suitable for that [16]. An on-line specific electrical conductivity monitor leaching system has been used to examine the leaching kinetics during water washing [17], which was a convenient real-time detecting method but lack of selectivity on elements. Furthermore, sintering dust exhibits strong hydrophobic property, dramatically inhibiting its wettability [18]. It was found that mechanical stirring and surfactants would enhance the wettability of sintering dust [19]. However, the effects of special surface characteristics, application of mechanical stirring and addition of surfactants on the leaching of chlorine have not been studied yet, which would be beneficial to removing chlorine from sintering dust.

Therefore, this study investigated the water leaching behavior and kinetics of chlorine with an on in-situ monitor leaching system based on chloride ion selective electrode. Both the effects of leaching temperatures, solid-liquid ratio and stirring speed on the leaching of chlorine in water were examined in detail. Furthermore, the effects of particle size and surfactant addition on the removal of chlorides were also analyzed. Besides, the leaching kinetics on the dissolution of chlorides was analyzed by Stumm's kinetic model and transition state theory. These analysis results are expected to provide some guidance for chlorine removal from iron ore sintering dust.

2. Materials and Methods

2.1. Materials and Reagents

The iron ore sintering dust samples were collected from the sintering plant at Panzhihua Iron & Steel (Group) Co., Ltd. in Panzhihua City, Sichuan Province, China. The elemental analysis of the samples was performed using X-ray fluorescence (XRF) spectrometry (PANalytical Axios mAX, Almelo, The Netherlands). Further, all the chemicals used in the experiments were AR/GR grade. Additionally, demineralized water was used throughout the experiments to leach metal chlorides and remove chlorine.

2.2. X-ray Diffraction Analysis

X-ray diffraction (XRD, X-Pert³ Power/Panalytical. B.V, Almelo, The Netherlands) was used to analyze the composition and crystal structure of the prepared samples at 40 kV, 100 mA for a Cu-target tube and a graphite monochromator. Standard procedures [20] were applied to prepare the samples for analysis by X-ray diffraction.

2.3. Granularity Analysis

A Malvern Mastersizer 2000 instrument (Malvern Instruments Ltd., Worcestershire, UK) with a detection range of 0.02~2000 µm was used to determine the size distribution of the original and ground sintering dust. A detector that converts the signal to a size distribution based on the volume detects the scattered light.

2.4. In-Situ Monitor Leaching Setup

An in-situ monitor leaching system based on chloride ion selective electrode was set up to examine the leaching behaviors of chlorine in real-time (Figure 1). A certain amount of iron ore sintering dust was added into deionized water in 1.0 L Bunsen beaker and stirred at different parameters including stirring speed (100, 300, and 600 rpm), solid-liquid ratio

(S/L ratio) (1/100, 1/50, and 1/25), bath temperature (25, 45, and 65 °C) and surfactant concentration (0%, 0.002%, 0.02%, and 0.2%). The concentration of chlorine in the solution was analyzed and recorded every 5 s to 1 min at the same time.

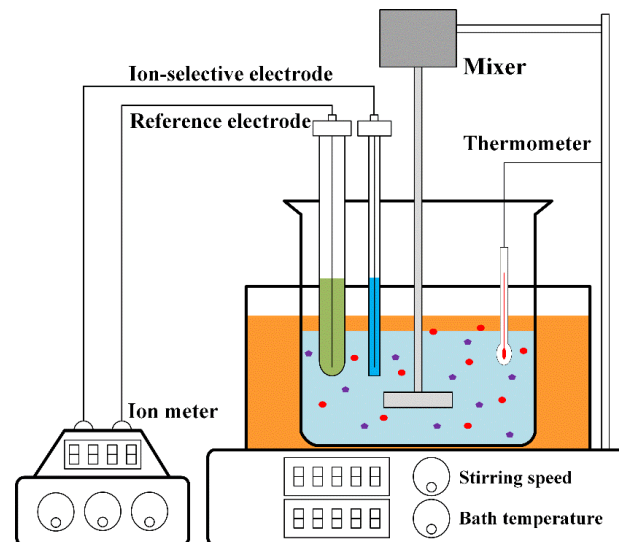


Figure 1. Diagram of the in-situ monitor leaching system.

2.5. Scanning Electron Microscopy Investigation

Scanning electron microscopy (SEM) was performed using a JEOL JSM-6490LV (Japan) equipped with an energy dispersive analyzer EDAX (EDS INCA x-act) to assess the characteristics of the samples [21]. The surface of the sample was measured after gold coating to improve the image quality.

2.6. Stumm's Kinetic Model

The Stumm's kinetic model [22,23] is employed to simulate the dissolution kinetics of chlorine in sintering dust. Its differential form is given in the following equation.

$$\frac{dC}{dt} = K(C_S - C_t)^n \quad (1)$$

where C_S (mol/L) and C_t (mol/L) are the dissolution concentration of chloride ion at equilibrium and time t , respectively. K represents the rate constant, which describes the dissolution rate of the sample. n represents the reaction order of dissolution in water. The nonlinear fitting of the test data via this model was calculated by Runge–Kutta differential equations. Considering using the dissolution rate of chlorine in water to replace the dissolution concentration of chloride ion would help to simplify the analysis procedure and clearly display all the necessary data, the differential form of Stumm's kinetic model could also be given in the following equation.

$$dD/dt = K(D_S - D_t)^n \quad (2)$$

where D_S and D_t represent the dissolution rate of chlorine at equilibrium and time t , respectively.

2.7. Transition State Theory Analysis

The temperature dependence could be used to estimate the apparent activation energy. The apparent activation energy of the system can be obtained from the Arrhenius expression [24].

$$K = Ae^{(-\frac{E_a}{RT})} \quad (3)$$

where T is the absolute temperature, K is the temperature-dependent rate constant. A is the pre-exponential factor, E_a is the apparent activation energy and R is the universal gas constant.

Based on transition state theory, the activation entropy and activation enthalpy could be calculated by the Eyring-Polanyi model [25]. Its equation has the form:

$$\ln \frac{K}{T} = -\frac{\Delta H^a}{R} \cdot \frac{1}{T} + \ln \frac{k_B}{h} + \frac{\Delta S^a}{R} \quad (4)$$

where ΔH^a is the activation enthalpy, k_B is the Boltzmann constant, h is the Planck's constant, ΔS^a is the activation entropy.

3. Results and Discussion

3.1. Properties of Iron Ore Sintering Dust

Previous studies [14,19] have examined the properties of iron ore sintering dust in detail. Considering that the aim of this study was the leaching kinetics of chlorine removing, properties of sintering dust were studied briefly.

3.1.1. Elemental Composition Analysis

The elemental composition of the sintering dust was analyzed by XRF spectrometry (Table 1). It can be found that the main elements in iron ore sintering dust sample is Cl, K, Pb and Fe.

Table 1. Main elements in iron ore sintering dust (mass fraction, %).

Elements	Cl	K	Na	Fe	Pb	Zn	S	Ca	O
Content	33.38	20.51	4.39	4.85	16.02	0.47	3.49	0.92	12.12

3.1.2. Phase Analysis

The major phases in sintering dust were studied by X-Ray Powder Diffraction (Figure 2). The results showed that the major phases of the sintering dust were sylvite, hematite and laurionite. Other phases included PbSO_4 , halite, gypsum, etc. These results were consistent with previous studies [26,27].

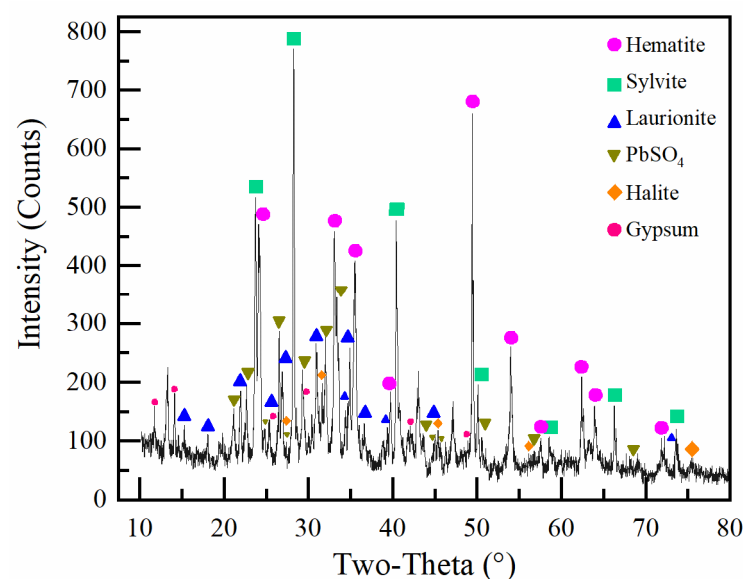


Figure 2. X-ray diffraction pattern of sintering dust.

3.1.3. Surface Morphology

The surface morphology of iron ore sintering dust was observed by SEM-EDS (Figure 3). As illustrated in Figure 3a, the size of sintering dust showed that most of the particles are porous agglomerates ranging from 5 to 35 μm with various shapes. These agglomerates are composites of fine individual dust ranging from 1 μm to 5 μm (Figure 3b). In addition, several cubic crystals were observed on the surface of larger particles or partly embedded in the agglomerates. Energy dispersive spectroscopy was employed to ascertain the content of the cubic crystals (Figure 3c). The content of the yellow cross mark was 45.76% Cl and 54.24% K, which inferred the cubic crystals were KCl grains. These results showed that the main chlorine-bearing component of the sintering dust was KCl, which overlapped on larger particles.

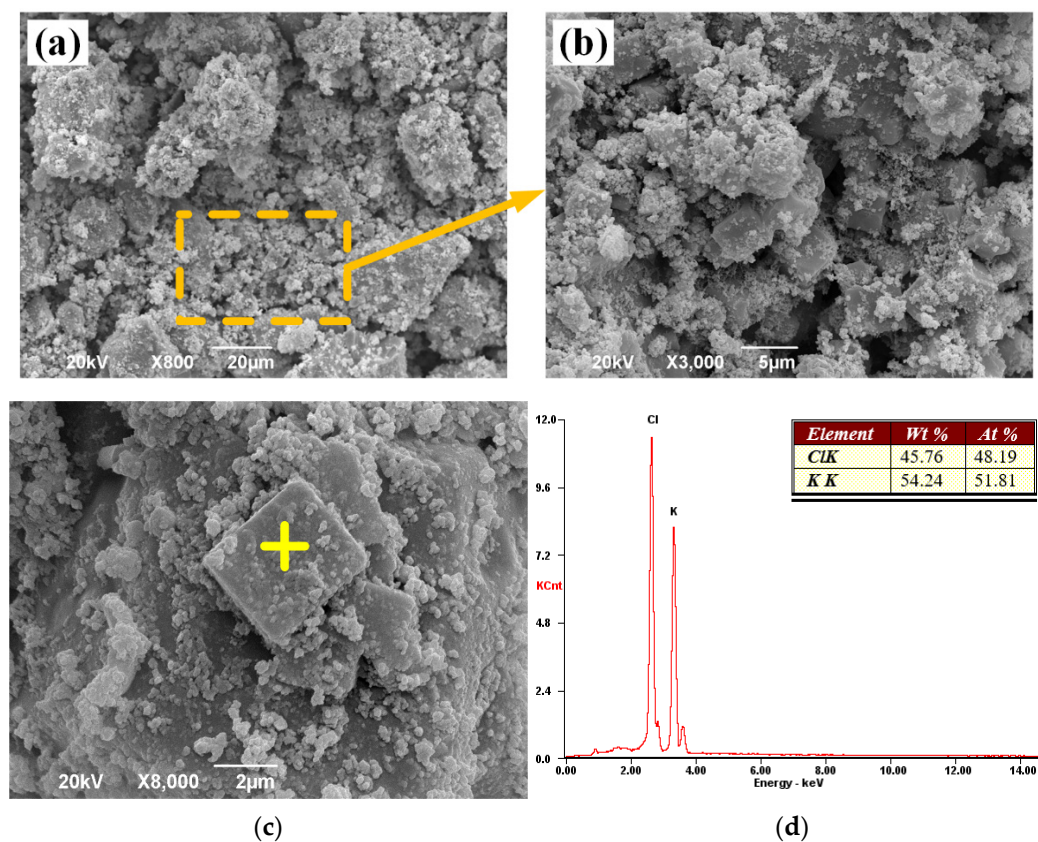


Figure 3. (a–c) SEM images and (d) EDS analysis of iron ore sintering dust.

3.2. Effects of Temperature and S/L Ratio

A special surface feature could be easily observed before and after mixing, showing the aggregates formed after being poured into the water and partly floating on the water surface (Figure 4). Further, the higher the stirring speed is, the less the amount of dust float on the water surface [18]. Previous studies on extracting potassium chloride showed that water leaching equilibrium could be reached within 5 min with a potassium recovery of 95% [17]. These results indicated that the hydrophobicity of sintering dust only has a limited influence on the leaching of potassium chloride under appropriate stirring speed. Thus, it could be inferred that water leaching could also easily remove most of the chlorine in the form of alkali chloride [11], which was also employed in this study.

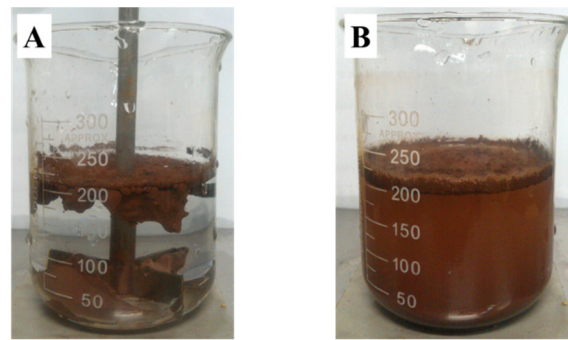


Figure 4. Photos of leaching before (A) and after (B) being stirred for 10 min at 600 rpm.

The leaching kinetics studies on the chlorine removal were started with the effects of temperature and solid to liquid ratio (S/L ratio) via the in-situ monitor leaching system. Due to the limitation of the maximum range of accurate measurement of chloride ion selective electrode, the experiments on the effects of solid to liquid ratio were conducted at 1:100, 1:50 and 1:25, respectively. Meanwhile, the original iron ore sintering dust samples were used, and the stirring speed was 600 rpm.

3.2.1. Solid to Liquid = 1:100

The chloride ion dissolution rates under solid to liquid ratio of 1:100 after water leaching for 15 min at 25 °C, 45 °C and 65 °C were 95.14%, 95.50% and 95.80%, respectively. The chlorine dissolution data can be satisfactorily simulated by Stumm's kinetic models (correlation coefficients $R^2 > 0.90$). These results indicated that the temperature only has a slight influence on the chloride final dissolution rate. However, it greatly affected the rate constant K (Figure 5), which increased more than 7 times as the temperature increases. The time for achieved 90% removal of chlorine was 12 min, 7 min and 3.5 min at 25 °C, 45 °C and 65 °C, respectively. Further, the dissolution of chlorine was relative slowly at 25 °C and almost reached its equilibrium after leaching for 15 min. Meanwhile, the reaction order n ranged from 0.44 to 1.06, which inferred that the influence of chloride ion concentration on the chlorine dissolution speed was very weak.

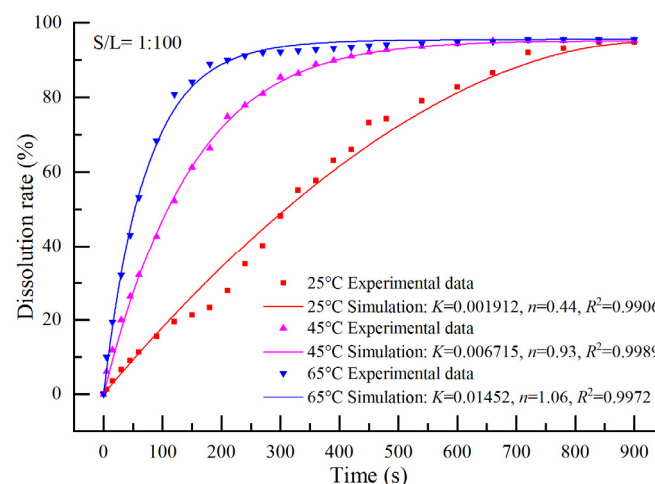


Figure 5. Effects of temperature on chloride ion dissolution rate with S/L ratio of 1:100 and stirring speed of 600 rpm.

3.2.2. Solid to Liquid = 1:50

The chloride ion dissolution rates under the solid to liquid ratio of 1:50 after water leaching for 15 min at 25 °C, 45 °C and 65 °C were 94.24%, 94.96% and 95.14%, respectively. The chlorine dissolving data exhibited a good fit for Stumm's kinetic models (correlation

coefficients $R^2 > 0.90$) [23]. These results also indicated that the effects of temperature on the final chloride dissolution rate were less, while the final chloride dissolution rates were a little bit lower than that of solid–liquid ratio of 1:100 at the same temperature. The temperature greatly affected the rate constant K (Figure 6) as well, which increased more than 5 times as the temperature increases. The time for achieved 90% removal of chlorine was 12 min, 8 min and 3.5 min at 25 °C, 45 °C and 65 °C, respectively, which was slightly longer than that for the solid to liquid ratio of 1:100. Further, only the dissolution of chlorine at 65 °C reached its equilibrium within leaching for 15 min. Meanwhile, the reaction order n ranged from 0.83 to 1.24, which inferred that the influence of chloride ion concentration on the chlorine dissolution speed increased than that of the solid to liquid ratio of 1:100.

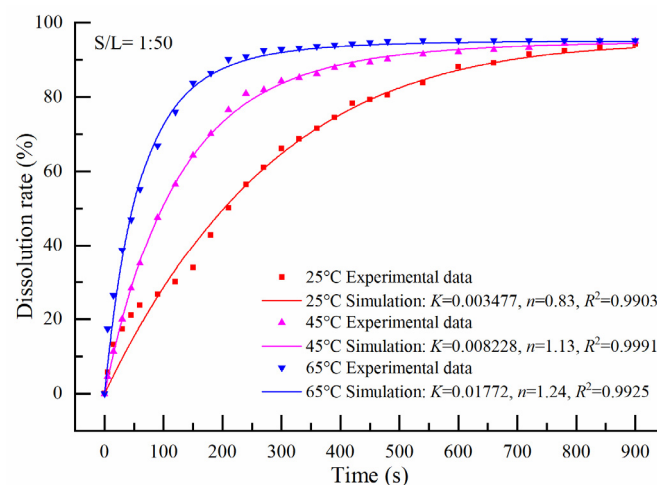


Figure 6. Effects of temperature on chloride ion dissolution rate with S/L ratio of 1:50 and stirring speed of 600 rpm.

3.2.3. Solid to Liquid = 1:25

The chloride ion dissolution rates under the solid to liquid ratio of 1:25 after water leaching for 15 min at 25 °C, 45 °C and 65 °C were 93.75%, 94.56% and 94.94%, respectively. The chlorine dissolving data also can be satisfactorily simulated by Stumm’s kinetic models (correlation coefficients $R^2 > 0.90$). These results still indicated that the influences of temperature on the final chloride dissolution rate were weak and the chloride removal rates were further lower than that of the solid–liquid ratio of 1:100 and 1:50 at the same temperature. When the temperature increased from 25 °C to 65 °C, the rate constant K improved twice (Figure 7). The time for achieved 90% removal of chlorine was 14 min, 2 min and 7.5 min at 25 °C, 45 °C and 65 °C, respectively, which was much longer than that for the solid to liquid ratio of 1:50 and 1:100. The dissolving of chlorine did not reach its equilibrium at each temperature within leaching for 15 min. Meanwhile, the reaction order n ranged from 1.46 to 1.56, which inferred that the chloride ion concentration would greatly affect the chlorine dissolution speed.

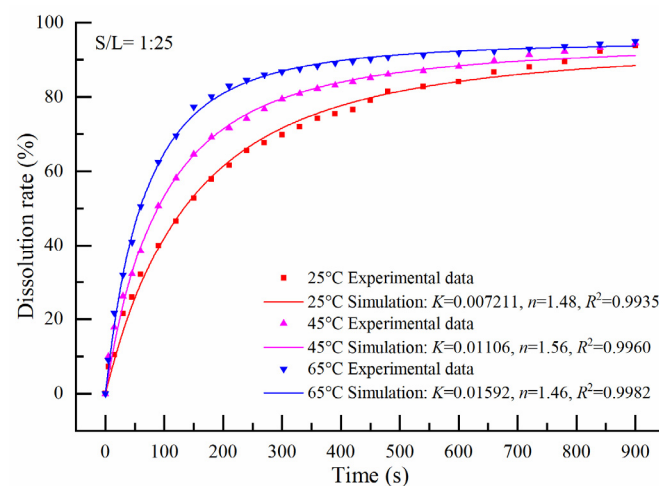


Figure 7. Effects of temperature on chloride ion dissolution rate with S/L ratio of 1:25 and stirring speed of 600 rpm.

3.2.4. Apparent Activation Energy Calculation

The dissolution kinetics of chlorine in sintering dust at different temperatures and S/L ratios exhibited a good fit to the Stumm's kinetic model. Based on these simulation results, the apparent activation energy was calculated by the Arrhenius equation [28], while the activation enthalpy and activation entropy were calculated by Eyring–Polanyi model (Table 2).

Table 2. Apparent activation energy, activation enthalpy and activation entropy calculation results.

S/L ratio	E_a (kJ/mol)	ΔH^a (kJ/mol)	ΔS^a (J/mol)
1:100	42.60	39.96	−162.37
1:50	34.10	31.46	−186.41
1:25	16.59	13.96	−239.06

Typically, the E_a value range for diffusion-controlled reactions is 8–25 kJ/mol in homogeneous solutions [29], while the E_a value of surface chemical reaction control [24,30] is >41.8 kJ/mol. In addition, the reaction that has an E_a between 25 and 41.8 kJ/mol is controlled by a combination of the surface chemical reaction and diffusion [31]. The apparent activation energy for the S/L ratio of 1:100, 1:50 and 1:25 were 42.60, 34.10 and 16.59 kJ/mol, respectively, which results demonstrated that the chlorine dissolution reaction rate control step changed from diffusion to surface chemical reaction as the S/L ratio increasing.

The apparent activation enthalpy for the S/L ratio of 1:100, 1:50 and 1:25 were 39.96, 31.46 and 13.96 kJ/mol, respectively. Both enthalpy's value was positive and small, which further illustrated that increasing temperature would accelerate the chlorine removing speed. Furthermore, it can be inferred that increasing the stirring speed and improving the surface reaction rate would benefit the water leaching of chlorides [32].

3.3. Effects of Stirring Speed

Stirring speed is one of the important factors affecting the dissolution process, especially for the diffusion-controlled reaction [33]. The leaching kinetics studies on the effects of stirring speed on chlorine removal were conducted with an S/L ratio of 1:50 at 25 °C via the in-situ monitor leaching system (Figure 8). The chloride ion dissolution rates after water leaching for 30 min with stirring speed of 100 rpm, 300 rpm and 600 rpm were 83.77%, 93.53% and 94.14%, respectively. The time for achieved 90% chlorine removal was 15 min and 12 min with stirring speed of 300 rpm and 600 rpm, respectively. Meanwhile, the rate constant K increased more than 2 times after the stirring speed increased from 100 rpm to 600 rpm. Whereas, the reaction order n only had minor changes, ranging from

0.98 to 1.28. These results indicated the stirring speed had much influence on the final chlorine dissolution rate and dissolving speed. Due to its strong hydrophobic surface feature, the iron ore sintering dust could not be fully dispersed and uniformly mixed with water to improve the chlorine dissolution with a low stirring speed. It further illustrated the removing chlorine process was partly controlled by diffusion with S/L of 1:50.

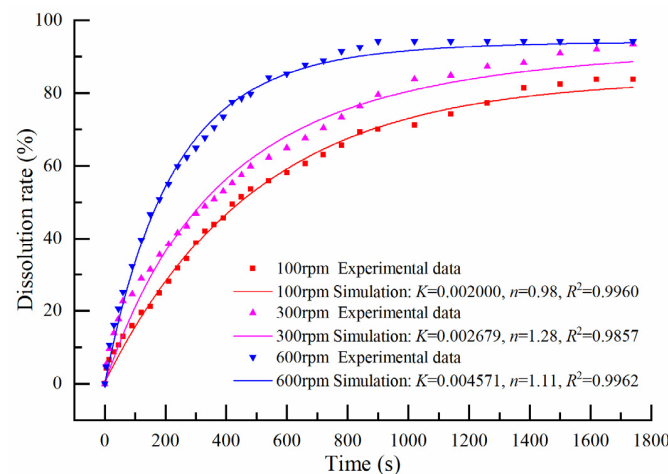


Figure 8. Effects of stirring speed on chloride ion dissolution rate with S/L ratio of 1:50 at 25 °C.

3.4. Effects of Particle Size

Decreasing the particle size would improve the leaching rate of chlorides [18]. To study the effects of particle size on the chlorine removal from iron ore sintering dust, a dry grinder was applied to mill the original samples for different periods. The volumetric mean diameter (D [3,4]) were 17.37 μm , 13.67 μm , 10.42 μm and 8.12 μm after being ground for 0 min, 2.5 min, 7.5 min and 25 min, respectively. The chlorine removing kinetics studies were conducted with these four samples with S/L ratio of 1:50 and stirring speed of 600 rpm at 25 °C via the in-site monitor leaching system (Figure 9). The chlorine dissolution rates after water leaching for 15 min were 94.14%, 95.36%, 95.77% and 95.78%, respectively, as the particle size decreases. The time for achieved 90% removal of chlorine for corresponding samples was 14 min, 11 min, 8 min and 7.5 min, respectively. Meanwhile, the rate constant K increased more than three times and the reaction order n increased from 1.15 to 1.54. These results indicated that reducing the particle size not only could benefit for the diffusion but also influence the surface chemical reaction since it would enlarge the specific surface area of sintering dust.

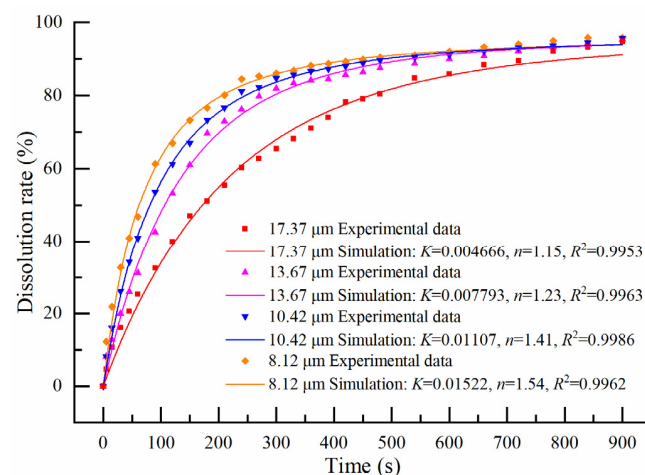


Figure 9. Effects of particle size on chloride ion dissolution rate with S/L ratio of 1:50 and stirring speed of 600 rpm at 25 °C.

3.5. Effects of Surfactant Addition

The addition of suitable concentration surfactant would sharply reduce the specific surface energy of particles, accelerate dissolution reaction increase leaching efficiencies [34,35]. In the previous study, a nonionic surfactant, Triton X-100 (TX-100), was used to enhance the wettability of sintering dust [19], which was efficient and economical. In this study, the effects of TX-100 on removing chlorine from sintering dust were examined with a concentration of 0, 0.002%, 0.02% and 0.2%, respectively (Figure 10). The chlorine dissolution rates after water leaching for 15 min were 94.14%, 94.39%, 95.98% and 96.70%, respectively, as the surfactant addition increased. The time for achieved 90% removal of chlorine for corresponding samples was 14 min, 12 min, 10 min and 3.5 min, respectively. The results indicated that the addition of surfactant all significantly promote chlorine dissolution kinetics. Especially when 0.2% TX-100 was employed, the rate constant K was enhanced by more than two times. Moreover, the reaction order n decreased from 1.15 to 0.95. It inferred the surface chemical-controlled dissolution reaction could significantly accelerate by the addition of appropriate surfactant.

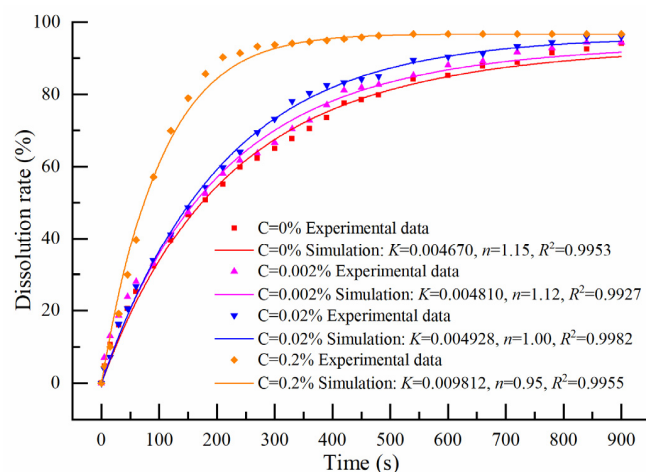


Figure 10. Effects of surfactant addition on chloride ion dissolution rate with S/L ratio of 1:50 and stirring speed of 600 rpm at 25 °C.

The effect of TX-100 on the contact angle between the mineral surface and liquid after touching for 20 s is presented in Figure 11. The contact angles are 95.4° (without surfactant), 89.0° (0.002% TX-100), 40.2° (0.002% TX-100) and 14.2° (0.002% TX-100), respectively. The result indicates that in the presence of surfactants, the contact angle between iron ore sintering dust and the leaching solution was gradually reduced, especially when the concentration was greater than 0.2%, which enhanced the contact between sintering dust particles and leaching liquid. As a result, the surface reaction rate was improved, which noticeably accelerated chlorine dissolution and removing efficiency.

3.6. SEM Examination of Insoluble Chlorides

According to the literature and the research of this paper, most of the chlorides in the iron ore sintering dust could be dissolved by water leaching, such as KCl, NaCl, PbCl₂ and ZnCl₂. However, the total dissolution rate of chlorine was limited to less than 97%. Overwhelming majority chlorides are soluble except silver chloride, some double salts and Friedel's salts [36]. Some double salts including lead hydroxide chloride and lead chloride carbonates were already found in electric arc furnace (EAF) dust [37]. Friedel's salt is the common name of the chlorinated lamellar double hydroxide of composition (3CaO·Al₂O₃·CaCl₂·10H₂O), which was found in the municipal solid waste incineration bottom ash [38]. In order to identify the insoluble chlorides in iron ore sintering dust, SEM-EDS was used to examine its leaching residue. The major elements in the dust were observed by SEM X-ray mapping (Figure 12). It can be easily seen that the distributions

of K and Na were disappeared. Moreover, Cl and Pb were distributed in the same way corresponding to acicular or flaky particles, while the distribution of O covered the area of Pb and Cl. This inferred laurionite (PbOHCl) presence in the residue, which was difficult to be dissolved by water. Thus, a promising way to further reduce the chlorine level of the iron ore sintering dust to make the product more acceptable to the sinter would be beneficiation or hydrometallurgy extraction of laurionite.

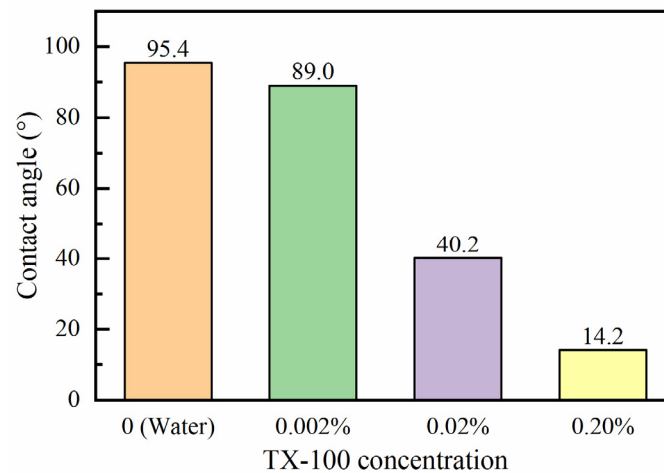


Figure 11. Contact angles between the mineral surface and different concentrations of TX-100 solutions after touching for 20 s.

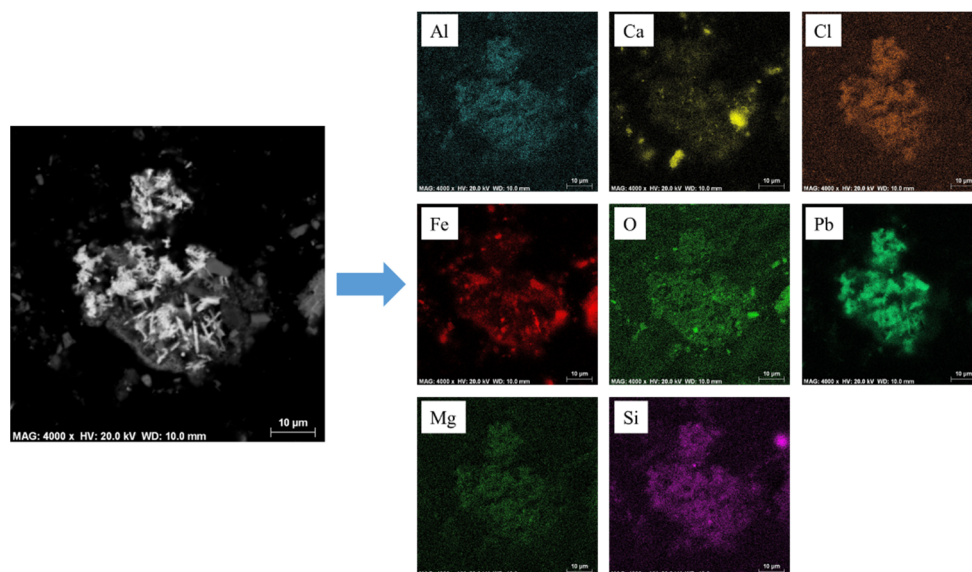


Figure 12. SEM-EDS examination on sintering dust leaching residue.

4. Conclusions

This study aimed to investigate the dissolution kinetics of chlorine removal from iron ore sintering dust. Both the effects of temperatures, solid-liquid ratio, stirring speed, particle size and surfactant addition on the removal of chlorine were examined in detail. The relative dissolution curves were analyzed by Stumm's kinetic model and transition state theory. The insoluble chlorides in the residue (such as silver chloride and PbOHCl) were investigated by SEM-EDS. Through the studies, the following results are highlighted.

- (1) Most of the sintering dust particles are porous agglomerates and the major chlorine-bearing substances in it were KCl , NaCl and PbOHCl . An in-situ monitor leaching system based on chloride ion selective electrode was designed to achieve real-time

detection on the chloride ion leaching behaviors, while the chlorine dissolution data exhibited a good fit to Stumm's kinetic models.

- (2) Based on the kinetics analysis and transition state theory calculation, the apparent activation energy of chlorine dissolution in sintering dust with an S/L ratio of 1:100, 1:50 and 1:25 were 42.60, 34.10 and 16.59 kJ/mol, respectively. It demonstrated that the dissolution was controlled by diffusion at low S/L ratio, while changed to controlled by surface chemical reaction as the S/L ratio increased. Meanwhile, increasing both temperature and stirring speed would accelerate the chlorine dissolving speed when the reaction was totally or partly controlled by diffusion.
- (3) Reducing the particle size and addition of 0.2% TX-100 would be a benefit for removing chlorine in sintering dust since they could cause a reduction in surface energy and acceleration of surface chemical reaction. Besides, the SEM-EDS examination inferred that the existence of laurionite limited the dissolution rate of chlorine less than 97%, while beneficiation or hydrometallurgy treatment was needed to further reduce the chlorine content of sintering dust to meet the demand of a sinter.

Author Contributions: Conceptualization, H.T. and L.W.; methodology, W.S.; validation, H.T., L.W. and W.S.; formal analysis, H.T. and Y.Y.; investigation, L.Z.; resources, H.H.; data curation, H.T. and L.W.; writing—original draft preparation, H.T.; writing—review and editing, L.W.; supervision, W.S.; funding acquisition, H.T., L.W. and W.S. All authors have read and agreed to the published version of the manuscript.

Funding: This research was funded by the National Natural Science Foundation of China (52004335), Natural Science Foundation of Hunan Province (2020JJ5747, 2020JJ5174), National Key R&D Program of China (2019YFC1907803, 2018YFC1901901) and Key Laboratory of Hunan Province for Clean and Efficient Utilization of Strategic Calcium-containing Mineral Resources (No. 2018TP1002).

Institutional Review Board Statement: Not applicable.

Informed Consent Statement: Not applicable.

Data Availability Statement: Not applicable.

Acknowledgments: We gratefully appreciate the financial support from the National Natural Science Foundation of China (52004335), Natural Science Foundation of Hunan Province (2020JJ5747, 2020JJ5174), National Key R&D Program of China (2019YFC1907803, 2018YFC1901901) and Key Laboratory of Hunan Province for Clean and Efficient Utilization of Strategic Calcium-containing Mineral Resources (No. 2018TP1002).

Conflicts of Interest: The authors declare no conflict of interest.

References

1. Lanzerstorfer, C.; Steiner, D. Characterization of sintering dust collected in the various fields of the electrostatic precipitator. *Environ. Technol.* **2016**, *37*, 1559–1567. [[CrossRef](#)]
2. Min, Y.; Liu, C.; Shi, P.; Qin, C.; Feng, Y.; Liu, B. Effects of the addition of municipal solid waste incineration fly ash on the behavior of polychlorinated dibenzo-p-dioxins and furans in the iron ore sintering process. *Waste Manag.* **2018**, *77*, 287–293. [[CrossRef](#)]
3. Chun, T.; Li, D.; Ning, C.; Wang, Z.; Long, H. *Characteristics and Control Technology of Fine Particulate Matter (PM) in Iron Ore Sintering*; Springer International Publishing: Cham, Switzerland, 2018.
4. Lanzerstorfer, C.; Bamberger-Strassmayr, B.; Pilz, K. Recycling of Blast Furnace Dust in the Iron Ore Sintering Process: Investigation of Coke Breeze Substitution and the Influence on Off-gas Emissions. *ISIJ Int.* **2015**, *55*, 758–764. [[CrossRef](#)]
5. Tang, H.; Sun, W.; Han, H. A novel method for comprehensive utilization of sintering dust. *Trans. Nonferrous Met. Soc. China* **2015**, *25*, 4192–4200. [[CrossRef](#)]
6. Chang, F.; Wu, S.; Zhang, J.; Kou, M.; Lu, H.; Wang, L. *Chemical, Physical and Morphological Changes of Sintering Dust by Mechanical Activation*; John Wiley & Sons, Inc.: Hoboken, NJ, USA, 2016; pp. 501–509.
7. Yu, Y.; Wang, Z.; Wei, H.; Li, Y.; Song, Q.; Zheng, Z. Separation and recovery of potassium chloride from sinter dust of a steel plant. *Ironmak. Steelmak.* **2019**, *46*, 193–198. [[CrossRef](#)]
8. Gan, M.; Ji, Z.; Fan, X.; Chen, X.; Zhou, Y.; Wang, G.; Tian, Y.; Jiang, T. Clean recycle and utilization of hazardous iron-bearing waste in iron ore sintering process. *J. Hazard. Mater.* **2018**, *353*, 381–392. [[CrossRef](#)]

9. Long, H.; Shi, Q.; Zhang, H.; Wei, R.; Chun, T.; Li, J. Application status and comparison of dioxin removal technologies for iron ore sintering process. *J. Iron Steel Res. Int.* **2018**, *25*, 357–365. [[CrossRef](#)]
10. Zhan, G.; Guo, Z. Basic properties of sintering dust from iron and steel plant and potassium recovery. *J. Environ. Sci.* **2013**, *25*, 1226–1234. [[CrossRef](#)]
11. She, X.; Wang, J.; Wang, G.; Xue, Q.; Zhang, X. Removal Mechanism of Zn, Pb and Alkalis from Metallurgical Dusts in Direct Reduction Process. *J. Iron Steel Res. Int.* **2014**, *21*, 488–495. [[CrossRef](#)]
12. Peng, C.; Zhang, F.; Guo, Z. Separation and Recovery of Potassium Chloride from Sintering Dust of Ironmaking Works. *ISIJ Int.* **2009**, *49*, 735–742. [[CrossRef](#)]
13. Şahin, F.Ç.; Derin, B.; Yücel, O. Chloride removal from zinc ash. *Scandinavian J. Metall.* **2000**, *29*, 224–230. [[CrossRef](#)]
14. Tang, H.; Zhao, L.; Sun, W.; Hu, Y.; Ji, X.; Han, H.; Guan, Q. Extraction of rubidium from respirable sintering dust. *Hydrometallurgy* **2018**, *175*, 144–149. [[CrossRef](#)]
15. Peng, C.; Guo, Z.; Zhang, F. Discovery of Potassium Chloride in the Sintering Dust by Chemical and Physical Characterization. *ISIJ Int.* **2008**, *48*, 1398–1403. [[CrossRef](#)]
16. Chen, W.; Chang, F.; Shen, Y.; Tsai, M.; Ko, C. Removal of chloride from MSWI fly ash. *J. Hazard. Mater.* **2012**, *237–238*, 116–120. [[CrossRef](#)]
17. Peng, C.; Guo, Z.; Zhang, F. Existing state of potassium chloride in agglomerated sintering dust and its water leaching kinetics. *Trans. Nonferrous Met. Soc. China* **2011**, *21*, 1847–1854. [[CrossRef](#)]
18. Zhan, G.; Guo, Z. Water leaching kinetics and recovery of potassium salt from sintering dust. *Trans. Nonferrous Met. Soc. China* **2013**, *23*, 3770–3779. [[CrossRef](#)]
19. Tang, H.; Zhao, L.; Sun, W.; Hu, Y.; Han, H. Surface characteristics and wettability enhancement of respirable sintering dust by nonionic surfactant. *Colloids Surf. A Physicochem. Eng. Asp.* **2016**, *509*, 323–333. [[CrossRef](#)]
20. Jin, J.; Liu, L.; Liu, R.; Wei, H.; Qian, G.; Zheng, J.; Xie, W.; Lin, F.; Xie, J. Preparation and thermal performance of binary fatty acid with diatomite as form-stable composite phase change material for cooling asphalt pavements. *Constr. Build. Mater.* **2019**, *226*, 616–624. [[CrossRef](#)]
21. Guan, Q.; Sun, W.; Guan, C.; Yu, W.; Zhu, X.; Khoso, S.A.; Wang, P.; Peng, W. Promotion of conversion activity of flue gas desulfurization gypsum into α -hemihydrate gypsum by calcination-hydration treatment. *J. Cent. South Univ.* **2019**, *26*, 3213–3224. [[CrossRef](#)]
22. Stumm, W.; Morgan, J.J. *Aquatic Chemistry An Introduction Emphasizing Chemical Equilibria in Natural Waters*; Wiley-Interscience: New York, NY, USA, 1970.
23. Cheng, P.; Chen, D.; Liu, H.; Zou, X.; Wu, Z.; Xie, J.; Qing, C.; Kong, D.; Chen, T. Synergetic effects of anhydrite and brucite-periclase materials on phosphate removal from aqueous solution. *J. Mol. Liq.* **2018**, *254*, 145–153. [[CrossRef](#)]
24. Alvarado-Macias, G.; Fuentes-Aceituno, J.C.; Nava-Alonso, F.; Lee, J. Silver leaching with the nitrite–copper novel system: A kinetic study. *Hydrometallurgy* **2016**, *160*, 98–105. [[CrossRef](#)]
25. Barsa, C.S.; Normand, M.D.; Peleg, M. On Models of the Temperature Effect on the Rate of Chemical Reactions and Biological Processes in Foods. *Food Eng. Rev.* **2012**, *4*, 191–202. [[CrossRef](#)]
26. Tang, H.; Jiang, F.; Hu, Y.; Han, H.; Wang, L.; Sun, W. Flotability of laurionite and its response to sulfidization flotation. *Miner. Eng.* **2020**, *148*, 106183. [[CrossRef](#)]
27. Zhan, G.; Guo, Z. Preparation of potassium salt with joint production of spherical calcium carbonate from sintering dust. *Trans. Nonferrous Met. Soc. China* **2015**, *25*, 628–639. [[CrossRef](#)]
28. Li, X.; Ye, Y.; Xue, S.; Jiang, J.; Wu, C.; Kong, X.; Hartley, W.; Li, Y. Leaching optimization and dissolution behavior of alkaline anions in bauxite residue. *Trans. Nonferrous Met. Soc. China* **2018**, *28*, 1248–1255. [[CrossRef](#)]
29. Zang, L.; Rodgers, M.A.J. Diffusion-Controlled Charge Transfer from Excited Ru(bpy)₃²⁺ into Nanosized TiO₂ Colloids Stabilized with EDTA. *J. Phys. Chem. B* **2000**, *104*, 468–474. [[CrossRef](#)]
30. Wang, H.H.; Li, G.Q.; Zhao, D.; Ma, J.H.; Yang, J. Dephosphorization of high phosphorus oolitic hematite by acid leaching and the leaching kinetics. *Hydrometallurgy* **2017**, *171*, 61–68. [[CrossRef](#)]
31. Xu, Y.; Jiang, T.; Wen, J.; Gao, H.; Wang, J.; Xue, X. Leaching kinetics of mechanically activated boron concentrate in a NaOH solution. *Hydrometallurgy* **2018**, *179*, 60–72. [[CrossRef](#)]
32. Ho, Y.; Harouna-Oumarou, H.A.; Fauduet, H.; Porte, C. Kinetics and model building of leaching of water-soluble compounds of Tilia sapwood. *Sep. Purif. Technol.* **2005**, *45*, 169–173. [[CrossRef](#)]
33. Zhu, Y.; Liao, Y.; Lv, W.; Liu, J.; Song, X.; Chen, L.; Wang, C.; Sels, B.F.; Ma, L. Complementing Vanillin and Cellulose Production by Oxidation of Lignocellulose with Stirring Control. *ACS Sustain. Chem. Eng.* **2020**, *8*, 2361–2374. [[CrossRef](#)]
34. Guan, R.; Yuan, X.; Wu, Z.; Wang, H.; Jiang, L.; Li, Y.; Zeng, G. Functionality of surfactants in waste-activated sludge treatment: A review. *Sci. Total Environ.* **2017**, *609*, 1433–1442. [[CrossRef](#)]
35. Liu, W.; Zhang, S.J.; Sun, F.; Liu, C. Catalytic Effect of a Combined Silver and Surfactant Catalyst on Cobalt Ore Bioleaching. *JOM* **2018**, *70*, 2819–2824. [[CrossRef](#)]
36. Ito, R.; Fujita, T.; Sadaki, J.; Matsumoto, Y.; Ahn, J. Removal of Chloride in Bottom Ash from the Industrial and Municipal Solid Waste Incinerators. *Int. J. Soc. Mater. Eng. Resour.* **2006**, *13*, 70–74. [[CrossRef](#)]

-
37. Chen, W.; Shen, Y.; Tsai, M.; Chang, F. Removal of chloride from electric arc furnace dust. *J. Hazard. Mater.* **2011**, *190*, 639–644. [[CrossRef](#)] [[PubMed](#)]
 38. Ahn, J.; Um, N.; Han, G.; You, K.; Cho, H. Effect of Carbonation in Removal of Chloride from Municipal Solid Waste Incineration Bottom Ash. *Geosystem Eng.* **2006**, *9*, 87–90. [[CrossRef](#)]